Applied Thermal Engineering 270 (2025) 126211

Contents lists available at ScienceDirect

Applied Thermal Engineering

journal homepage: www.elsevier.com/locate/apthermeng

Research Paper

A novel photo-thermal synergistic catalytic method for degradation of waste Hydrofluorocarbons as greenhouse gases

Tianhao Wang, Jiajie Li, Datong Xie, Hongjing Miao, Lin Shi, Xiaoye Dai *

Key Laboratory for Thermal Science and Power Engineering of Ministry of Education, Key Laboratory for CO2 Utilization and Reduction Technology of Beijing, Department of Energy and Power Engineering, Tsinghua University, Beijing 100084, China

ARTICLE INFO

Keywords:
Hydrofluorocarbon
Destruction technology
Photo-thermal synergistic catalysis
Reaction kinetic analysis
Deactivation mechanism

ABSTRACT

Hydrofluorocarbons (HFCs) with high Global Warming Potential (GWP) values have great effects on global warming problems. The current HFCs commercial destruction technologies have extremely high energy consumption and cost. This paper proposes a novel photo-thermal synergistic catalysis method for the degradation of Hydrofluorocarbon (HFC) refrigerants, with HFC134a as the test substance. The method demonstrated a significantly higher reaction rate compared to conventional thermocatalysis and photocatalysis methods under relatively mild conditions. Complete mineralization of HFC134a to CO_2 was achieved. The influence of various experimental conditions, including different catalysts, temperatures, light intensities, and reaction components, was systematically analyzed. The results showed that the photo-thermal method outperformed other catalytic methods, making it a promising alternative for waste HFC destruction. Furthermore, a kinetic model of the degradation process was established, revealing first-order kinetics and a low activation energy of 22.3 kJ·mol^{-1}, which was much lower than that of thermal decomposition. The catalyst characterization results showed that $TiOF_2$ was formed during the reaction, indicating the importance of catalyst anticorrosion and regeneration for ensuring the long-term stability of the system. This study provides a comprehensive understanding of the reaction characteristics and proposes an efficient, low-energy solution for the destruction of waste HFCs.

1. Introduction

Refrigeration and air conditioning technology is essential for modern industrial production and comfortable daily life. The synthetic refrigerants play an important role in the progress of refrigeration and air conditioning technology with their excellent thermodynamic performance. However, some synthetic refrigerants can cause serious environmental problems. Chlorofluorocarbon (CFC) and hydrochlorofluorocarbon (HCFC) refrigerants were found to cause serious damage to the ozone layer. Thus, the production and usage of CFCs and HCFCs were restricted by the Montreal Protocol in 1987 [1]. Hydrofluorocarbon (HFC) refrigerants were then developed as the substitute for CFC and HCFC refrigerants, which had no effect on the ozone layer [2,3]. Global warming has become a global environmental problem recently. The high Global Warming Potential (GWP) values of HFCs have attracted more attention and they have been considered as one of the main non-CO_2 greenhouse gases, so the restriction for HFCs is also on the agenda [4]. The phase-out schedule of HFCs has been proposed by the Kigali Amendment to the Montreal Protocol in 2016, which can make a big contribution to the target for global warming mitigation. [5].

HFCs are the main commercial synthetic refrigerants with the production yield of approximate million tons in recent years. Thus, there will be a huge amount of waste HFCs according to the phase-out schedule in the next few decades [6]. The waste refrigerants must be destructed to avoid the greenhouse effect, so the destruction method of waste refrigerants has attracted wide attention around the world. Since 2008, about 155 destruction facilities have been operated in 28 countries [7]. The existing mature refrigerant destruction treatment technologies mainly include incineration and plasma technologies [8]. Incineration technologies utilize the controlled flame to destroy waste refrigerants in industrial devices with temperatures generally higher than 1000 °C. Plasma technologies utilize plasma with temperatures of 4700-19700 °C to destroy waste refrigerants, which is created from the discharge of a large electric current or in a magnetic field [7]. The main characteristics of these methods can be summarized as the pyrolysis of waste refrigerants at high temperatures (higher than 1000 °C), which lead to the advantages including the simple reaction mechanism, easy control of reaction conditions, and higher destruction rates. However,

* Corresponding author.
E-mail address: daixy@mail.tsinghua.edu.cn (X. Dai).

https://doi.org/10.1016/j.applthermaleng.2025.126211
Received 12 October 2024; Received in revised form 21 January 2025; Accepted 10 March 2025
Available online 13 March 2025

the extremely high temperatures also lead to high energy consumption, high cost, and harmful products (such as trifluoroacetic acid and dioxins, etc.) [9–11]. For destroying the huge amount of the waste HFCs, a new refrigerant destruction technology with low energy consumption, mild conditions and strong processing capacity is needed.

In recent studies, catalytic destruction methods, including thermocatalysis decomposition and photocatalysis degradation, have attracted more attention. In terms of thermocatalysis decomposition researches, Roh et al. [12] found that HFC134a could realize complete decomposition when the reaction temperature was above 950 °C, the residence time of the reaction gas was more than 4 s, and the stoichiometric ratio of oxygen to HFC134a was 1.5. Han et al. [13] compared the thermocatalysis decomposition of HFC134a at 300~600 °C with different catalysts. The catalyst γ-Al_2O_3 was found to have a good catalytic effect, but it was easy to be corroded and deactivated by HF generated in the reaction. Kinds of by-products were also observed during the decomposition. Swamidoss et al. [14] used an Mg/Al_2O_3 catalyst to conduct thermal catalytic decomposition of HFC134a at 600 °C, and the degradation rate exceeded 90 %. However, a large number of TrFE by-products were produced and the corrosion of the catalyst was also observed. Jeong et al. [15] improved the efficiency of HFC134a decomposition by combining MgO with γ-Al_2O_3 at 600 °C, and extended the catalyst lifetime more effectively.

In terms of the studies of photocatalysis degradation, Sangchakr et al. [16] selected TiO_2 as a photocatalyst to compare the photocatalysis degradation of HFC152a under different wavelength conditions with the degradation products analyzed. Kutsuna et al. [17] compared different oxides as photocatalysts, such as TiO_2, ZnO and Fe_2O_3, for the photocatalytic degradation of CFC11. The experimental results showed all the selected photocatalysts had obvious photocatalysis effects on the degradation of CFC11. Wylie et al. [18] analyzed the photocatalytic degradation of various HFCs and CFCs and found that the photocatalytic reaction occurred only when the wavelength was less than 300 nm. Tennakone et al. [19] used TiO_2 as the catalyst to degrade flowing CFCs and mineralize them into CO_2, HF and Cl_2 and other by-products. The results showed that the reaction was triggered by oxygen-containing free radicals generated on the surface of the catalyst.

In summary, the thermocatalysis and photocatalysis degradation methods can significantly decrease reaction temperatures compared with incineration and plasma technologies. So catalytic destruction methods may lead to lower energy consumption and cost than incineration and plasma methods. However, there are still some problems which impede the commercial application of catalytic destruction methods. For thermocatalysis decomposition method, the catalyst inactivation and by-product problems in long react periods cannot be ignored and have big negative effects on the decomposition efficiency. For photocatalysis degradation method, the previous studies mainly focus on the catalyst screening at room temperature. So the concentrations of refrigerants and degradation rates are very small, which do not match the demands for industrial destruction technologies.

Compared to the single thermocatalysis and photocatalysis, photothermal synergistic catalysis technology combines the effects of light and heat, utilizing a coupling enhancement mechanism to achieve efficient reactions at moderate to low temperatures. This technology has been widely applied in the degradation of VOCs, treatment of water pollutants, CO_2 reduction, and water splitting [20–23]. However, the degradation of HFC134a requires high concentration, far exceeding the degradation levels of a few ppm typically achieved in existing photothermal synergistic catalytic pollutant degradation systems. Moreover, the degradation of HFC134a primarily involves breaking C—F bonds, which has a much stronger bond energy compared to the C—C or C—H bonds in the degradation of other pollutant or VOCs. Additionally, the degradation of HFC134a may produce HF, leading to a highly corrosive reaction system. Therefore, it is necessary to explore the specific characteristics of photo-thermal synergistic degradation of HFC134a.

Thus, a novel photo-thermal synergistic catalysis method for degradation of waste HFCs was proposed in this paper, which can degrade high concentrations of HFC134a by cleaving C-F bonds. Light and temperature conditions were provided at the same time for the degradation reactions of HFCs. HFC134a was chosen as the test refrigerant sample, which was one of main commercial HFCs with largest production. A photo-thermal synergistic catalysis experiment system was designed as shown in Section 2 of this paper. The feasibility of photo-thermal synergistic catalytic method was first verified. Then the characteristics of photo-thermal synergistic catalytic reaction and catalyst, the kinetic analysis, and the reaction mechanism were analyzed in Section 3.

2. Experimental method

2.1. Experimental materials

To conduct degradation tests of HFC134a, the gas composition generally requires HFC134a, O_2, and other components. The HFC134a refrigerant used in this paper was made by Dongyue company. O_2, He and Ar were made by Haipu company.

The effect of catalytic materials on the photothermal degradation of HFC134a remains unclear. Therefore, several different catalysts were selected for a brief comparison. Among them, anatase TiO_2, P25 TiO_2, and wurtzite ZnO were all sourced from McLin Company. The preparation of g-C_3N_4 followed the method described in reference [24], where 10 g of urea was heated to 550 °C at a rate of 5 °C per minute and calcined for 4 h to obtain the catalyst. The preparation of monoclinic monazite $BiPO_4$ followed the method outlined in reference [25], where 3 mmol of $Bi(NO_3)_3{\cdot}6H_2O$ and 3 mmol of $Na_3PO_4{\cdot}12H_2O$ were dispersed in 30 mL of deionized water and subjected to hydrothermal treatment at 180 °C for 72 h. The precipitate was then washed, centrifuged, and dried to obtain the catalyst. The information of catalysts was shown in Table 1:

X-ray diffraction (XRD) patterns were acquired on a Model D/max-rC X-ray diffractometer by using a Cu Kα radiation source. The purchased or synthesized materials were characterized by XRD, and the results are shown in Fig. 1. As can be seen, the structures of the purchased or synthesized catalysts are generally in agreement with those reported in the literature.

The morphology of the prepared samples was characterized by scanning electron microscopy (SEM, Hitachi S5500). Fig. 2 presents the SEM images of several catalysts. It can be observed that, except for g-C_3N_4, which maintains a bulk morphology, the other catalysts exhibit a nanoparticle morphology.

2.2. Experimental system

A schematic diagram of the experimental system is shown in Fig. 3. A gas-phase photo-thermal synergistic catalytic reactor made of stainless steel was designed with a volume of 54 mL for the experiments. The common materials for reactor light window are quartz glass and polyfluoroalkoxy (PFA), however, these materials can be easily corroded or aged by the HF in the reaction products under long-term photo-thermal synergistic catalysis conditions. Thus, CaF_2 glass was used as a light window material in this experimental system to ensure long-term stable light transmittance under photo-thermal conditions and HF corrosion.

Table 1
Types and Sources of catalysts.

Catalyst	Information	Source
TiO_2	Anatase TiO_2	Maclin
TiO_2	Anatase TiO2	Guoyao
P25	Rutile TiO_2 and anatase TiO_2 mixed	Maclin
P25	Rutile TiO_2 and anatase TiO_2 mixed	Jiuidng
ZnO	Wurtzite ZnO	Maclin
g-C_3N_4	Graphite C_3N_4	Prepared based on reference[24]
$BiPO_4$	Monoclinic monazite $BiPO_4$	Prepared based on reference[25]

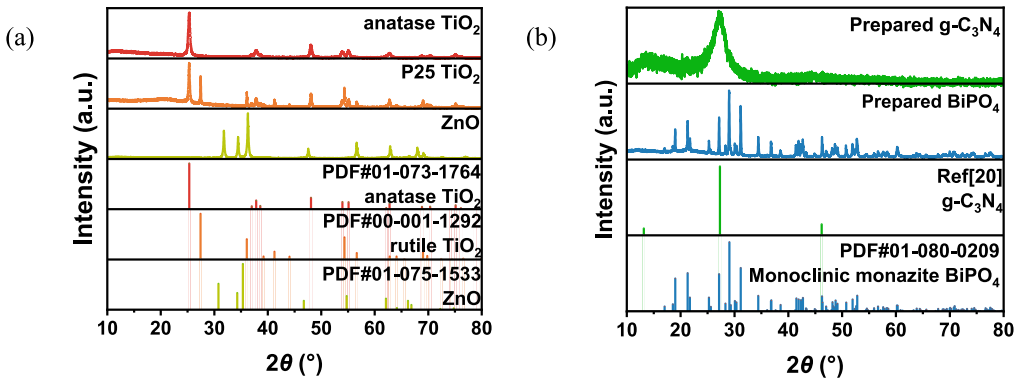

Fig. 1. XRD patterns of (a) anatase TiO_2, P25 TiO_2 and ZnO; (b) g-C_3N_4 and $BiPO_4$.

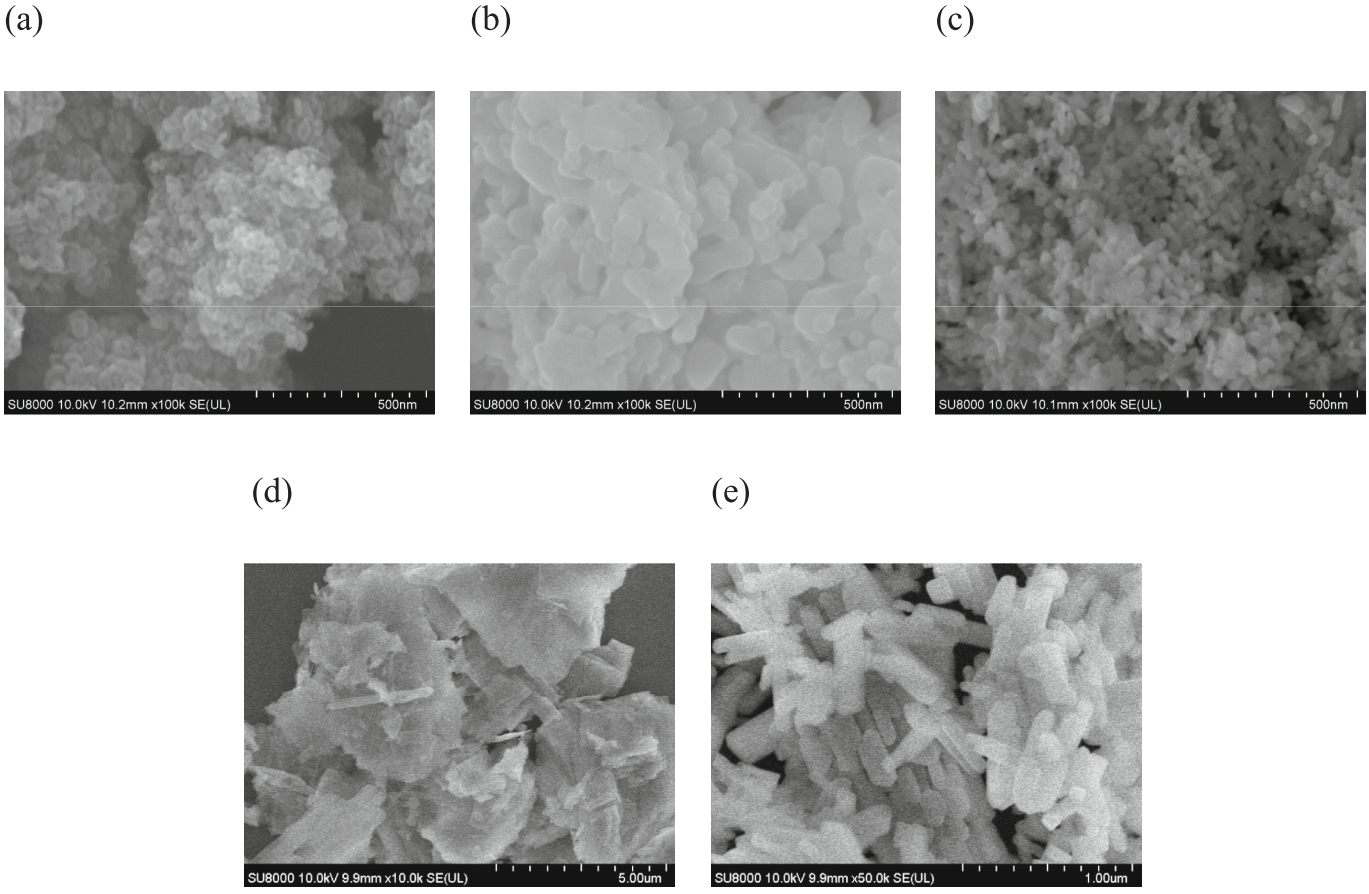

Fig. 2. SEM images of (a) anatase TiO_2 (100 k); (b)P25 TiO_2 (100 k); (c)ZnO (100 k); (d) g-C_3N_4 (10 k); (e) $BiPO_4$ (50 k).

The reactor was equipped with inlet and outlet connections for charging and discharging reactant gases. The temperature of the reactor was controlled by the heating plate with a maximum temperature of 240 °C, and a K-type thermocouple with the accuracy of ± 1.5 °C was inserted under the catalyst for the temperature test. The light was provided by a Perfectlight 300 W Xe lamp with the radiation intensity between 0.5 W/cm^2 and 1.20 W/cm^2. The light intensity was tested by a Thorlabs S425C power sensor with 5 % measurement uncertainty. The reactor was sealed with a fluorine rubber ring capable of 300 °C. The tightness of the reactor was verified by a YB80A digital gauge with the accuracy of 0.1 % FS. The reactor was injected to a gauge pressure of 100 kPa at 120 °C. After maintaining this condition for 24 h, the pressure change was less than 2 kPa, indicating that the reactor has good sealing performance. The concentrations of the reaction products were analyzed using an Agilent 7890B gas chromatograph (GC) with a thermal conductivity detector, a Porpark N column and high-purity Ar as the carrier gas.

The catalyst of 1 g was deposited in the bottom of the reactor during each reaction to ensure that the bottom was completely covered by the catalyst before the test, which can also ensure that probable corrosion will not influence the experiment result (since the adequate amount of catalyst). In each experiment, the reactor was first vacuumized, then 6 mL HFC134a and a certain mass of O_2 were injected by an injector into the reactor. Ar was supplemented to ensure that the reactor was in a slightly positive pressure state of 0.11~0.12 MPa. Gas was mixed at least 1 h to make sure the uniformity of concentration field. The reaction was proceeded with the set temperature and light intensity. The reaction products were analyzed by the GC after a certain reaction period. A 500 μL microinjector was used for the GC test. To improve the measurement

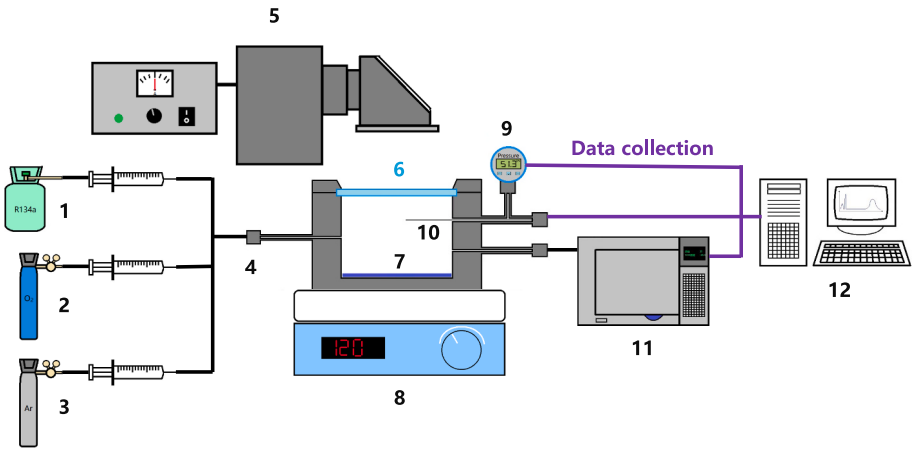

Fig. 3. Schematic diagram of the experimental system. 1-R134a; 2-O_2; 3-Ar; 4-Gas injection inlet; 5-Xe lamp system; 6-CaF_2 glass; 7-Catalyst; 8-Heating plate; 9-Pressure gauge; 10-Thermaocouple; 11-GC system; 12-Data collection computer.

accuracy, a small amount (1∼3 mL) of He was injected into the reactor, and the gas concentration was calculated by the internal standard method.

To confirm the measurement deviation of this experimental system, 5 repeated tests were conducted at 120 °C and 0.75 W/cm^2, as shown in Fig. S1. The results showed that the maximum deviation of the repeated tests was smaller than 5 %, which verified the accuracy of his experimental system.

For catalyst characterization, X-ray photoelectron spectroscopy (XPS) measurements were performed using a Thermo VG Scientific ESCALAB 250 spectrometer with an Al Kα radiator. A Fourier transform infrared spectrum (FTIR) analyzer (Protea Co., Ltd., Model# AFS-B2T, UK) and gas chromatography-mass spectrum (GC-MS) with an HP PLOT (Agilent, 19091P-Q04) column were employed to measure the composition of the reaction products.

3. Results & Discussion

3.1. Characteristics of the photo-thermal synergistic catalytic degradation reaction

To verify the effect of the catalyst on HFC134a degradation, different degradation experiments in the condition of 120 °C and 0.75 W/cm^2 light were compared with no catalyst and typical catalysts including anatase TiO_2, P25-TiO_2, ZnO, g-C_3N_4 and $BiPO_4$. As shown in Fig. 4a, no obvious degradation of HFC134a occurred without a catalyst. With the addition of catalysts, the degradation of HFC134a occurred obviously, while the degradation reaction rate with TiO_2 was much bigger than those with other catalysts. These results indicated that the catalyst played a crucial role in the photo-thermal synergistic catalytic degradation of HFC134a and had an important impact on the degradation efficiency.

Furthermore, several kinds of TiO_2 catalysts was tested, including rutile TiO_2 produced by Maclin, P25 TiO_2 produced by Jiuding and anatase TiO_2 produced by Guoyao. The XRD patterns of these catalysts were shown in Fig. S2a. It is evident that the P25 catalyst provided by Jiuding Company has a higher proportion of rutile phase than Maclin P25.

Fig. S2b presented the degradation rates for TiO_2 catalysts. As shown, compared to anatase TiO_2, rutile TiO_2 showed no catalytic activity for the degradation of HFC134a. Jiuding P25 also showed very low degradation activities, especially lower than Maclin P25, which coud probably be attributed to the weaker photocatalytic activity of the rutile phase with respect to HFC134a. Fig. S2b also presented the degradation results for anatase TiO_2 from Guoyao company. Although this anatase TiO_2 had a lower activity than MacLin's anatase TiO_2, it still exhibited higher activity than several P25 catalysts.

In summary, based on the analysis above, it is clear that anatase TiO_2 is more suitable for the photothermal catalytic degradation of HFCs. Thus, anatase TiO_2 produced by Maclin which have a big degradation reaction rate was used as the catalyst for the other tests in this paper.

To verify the synergistic effect of thermocatalysis and photocatalysis, the degradation experiments of HFC134a were tested with three different conditions: no light at 120 °C, 0.75 W/cm^2 light at room temperature, and 0.75 W/cm^2 light at 120 °C. The results are shown in Fig. 4b. No obvious degradation was detected in the condition of 120 °C without light within 120 min. Under room temperature with 0.75 W/cm^2 light intensity, less than 20 % of the initial HFC134a was degraded in 120 min. However, under 120 °C with 0.75 W/cm^2 light intensity, over 98 % of HFC134a degradation was achieved within 120 min, which was significantly faster than that under 0.75 W/cm^2 light at room temperature. These results indicated that the reaction rate of photo-

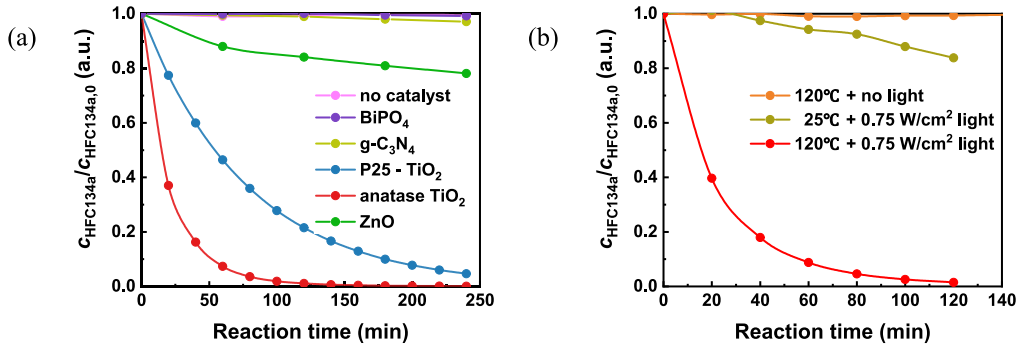

Fig. 4. (a) Degradation of HFC134a with different catalysts; (b) Comparison of degradation in different conditions.

thermal catalysis was much higher than those of thermocatalysis and photocatalysis respectively, and also much higher the simple sum of the thermal degradation at 120 °C or the degradation rate under light irradiation at room temperature, indicating the presence of a synergistic effect in the photothermal catalytic degradation of HFC134a. Furthermore, based on the performance of individual light or heat degradation, this synergistic effect might arise from thermally assisted photocatalysis, where the migration of charge carriers accelerates with increasing temperature, resulting in an exponential increase in the reaction rate.

Meanwhile, the complete degradation of HFC134a could be easily realized in the mild conditions using photo-thermal catalytic method instead of at a high temperature of nearly 1000 °C. Therefore, photo-thermal synergistic catalysis is a feasible and valuable method for refrigerant degradation.

Fig. 5a shows the relationship between the degraded concentration of HFC134a and the concentration of CO_2 in the products in the experiments with 120 °C and 0.75 W/cm^2 light. The results showed that the degraded concentration of HFC134a and concentration of CO_2 in the products had a good linear relationship, which indicated that the mineralization ratio was almost constant throughout the reaction process. The slope of the straight line obtained by linear fitting in Fig. 5a was about 1.99, indicating that the mineralization ratio was 99.64 %. These results indicated that photo-thermal synergistic catalysis could achieve almost complete mineralization of HFC134a with anatase TiO_2 as the catalyst.

Fig. 5b shows the curve of the relationship between the degraded concentration of HFC134a and the reduced concentration of O_2 during the repeated experiments under the condition of 120 °C and 0.75 W/cm^2 light. The results showed that the relationship between HFC134a concentration reduction and O_2 concentration reduction also had good linearity. The slope of the straight line obtained by linear fitting was about 1.49 in Fig. 5b. The results indicated that the degradation of 1 mol of HFC134a in this experimental system needed approximately 1.5 mol of O_2, and this value was almost constant during the progress of the reaction.

Fig. 6a shows the degradation reaction of HFC134a with different O_2 concentrations under the condition of 120 °C and 0.75 W/cm^2 light. When $c_{O2.0}/c_{HFC134a,0}$ was bigger than 1.5, the degradation rate effectively did not vary with the changes of $c_{O2.0}$. When $c_{O2.0}/c_{HFC134a,0}$ was smaller than 1.5, O_2 was insufficient for the degradation reaction. As shown in Fig. 6b, the degradation reaction of HFC134a would stop when the oxygen in the reaction system was used up. The concentration reductions of HFC134a when degradation reactions stopped and the initial oxygen concentration are listed in Table S1. The results showed that the degradation of 1 mol of HFC134a consumed approximately 1.5 mol of O_2, which was consistent with the conclusion in Fig. 5b.

FTIR and GC-MS tests were performed on the remaining gas after 120 min of reaction. Fig. 7a shows the FTIR spectra of the gas sample before and after the reaction. The peaks of CO_2 and H_2O appeared after the reaction, while the peak of HFC134a was greatly weakened. The comparison of FTIR spectra before and after the reaction showed that the vibration absorption peaks of HFC134a in the range about 1000–1500 cm^{-1} only exhibit changes in intensity, with no changes in the relative ratios of the vibration absorption peaks corresponding to C—F, C—H and C—C bonds, also no shift of the peaks were observed, as shown in Fig. S3a. FTIR spectra of CHF_3 or C_2HF_3 which usually appeared as byproduct durring HFC134a degradation [26] were shown in Fig. S3b. Comparing with the these, no new peaks such as C═C vibration or shifted C—H and C—F bonds vibration was observed in FTIR spectra of reacted gas. The FTIR results probably indicate that no other organic substance was generated, proving the complete mineralization of HFC134a.

Fig. 7b shows the MS results of the gas after the reaction. Three peaks appeared at approximately 1.9 min, 2.9 min and 9.3 min. The peak near 1.9 min was attributed to air. By comparing the peaks near 2.9 min and 9.3 min with the cards in the card library, it is found that the peak at 2.9 min was attributed to CO_2, and the peak near 9.3 min was attributed to HFC134a, as shown in Fig. S4a and Fig. S4b. No other products except HFC134a and CO_2 were detected by MS, indicating that no by-product was produced during the reaction. The MS results also verified that HFC134a was effectively completely mineralized by the photo-thermal synergistic catalytic degradation method.

3.2. Kinetic analysis of the degradation reaction

To investigate the reaction series of the degradation reaction, the relationship between $\ln(c_{HFC134a}/c_{HFC134a,0})$ and the reaction time at 120 °C is shown in Fig. 8a. The results showed that $\ln(c_{HFC134a}/c_{HFC134a,0})$ had a good linear relationship with reaction time, indicating that the reaction was a first-order reaction for HFC134a. Therefore, the degradation reaction rate can be calculated using Eq. (1).

$$d(c_{HFC134a}/c_{HFC134a,0})/dt = -k\cdot(c_{HFC134a}/c_{HFC134a,0}) \quad (1)$$

where k is the reaction rate constant and equals the slope of the $\ln(c_{HFC134a}/c_{HFC134a,0})$–$t$ curve.

Fig. 8b shows the degradation data under various temperature conditions, showing that the degradation rate gradually increased with increasing temperatures. The relationship of $\ln(c_{HFC134a}/c_{HFC134a,0})$ and reaction time at different temperatures is shown in Fig. S5, demonstrating good linearity within the temperature range of 80~160 °C. According to the Arrhenius formula (Eq. (2)), there is a linear relationship between $\ln k$ and $1/T$ (Eq. (3)). Therefore, the $c_{HFC134a}$ could be calculated by the apparent kinetics model as Eq. (4).

$$k = A_0\cdot\exp(-E_a/RT) \quad (2)$$

$$\ln k = (-E_a/R)\cdot(1/T) + \ln A_0 \quad (3)$$

$$c_{HFC134a} = c_{HFC134a,0}\cdot\exp(-A_0\cdot\exp(-E_a/RT)) \quad (4)$$

On the basis of this apparent kinetics model, the activation energy E_a of the reaction was calculated to be 22.3 kJ/mol and the pre-exponential factor A_0 was calculated to be 35.12 min^{-1}., which used gradient

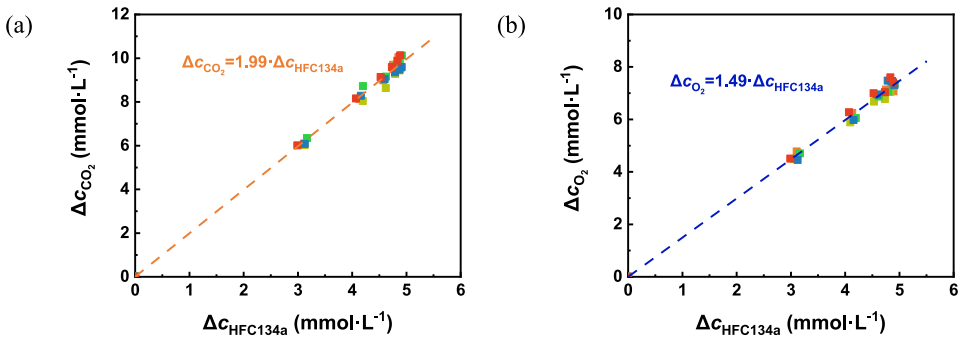

Fig. 5. Relationship between the degraded concentration of HFC134a and (a) concentration of CO_2 in the products; (b) reduced concentration of O_2.

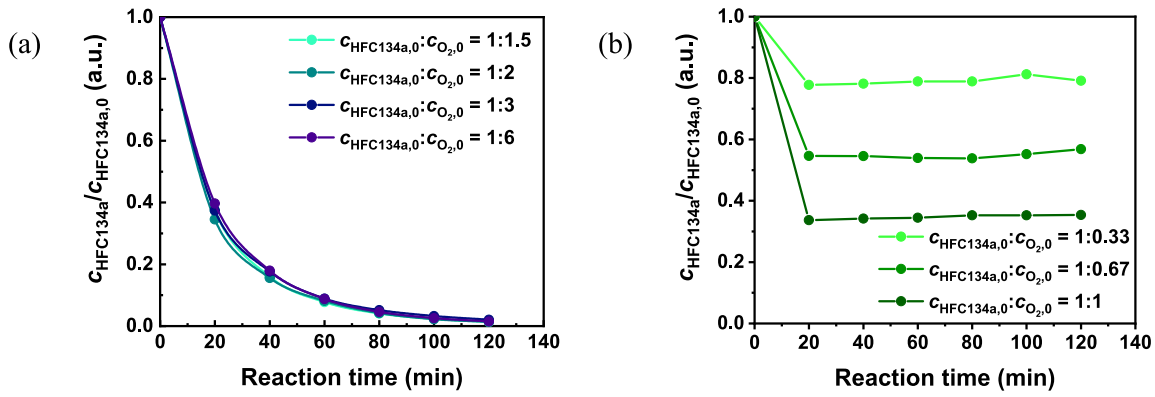

Fig. 6. Influence of $c_{O2.0}/c_{HFC134a,0}$ (a) $c_{O2.0}/c_{HFC134a,0} \geq 1.5$; (b) $c_{O2.0}/c_{HFC134a,0} < 1.5$.

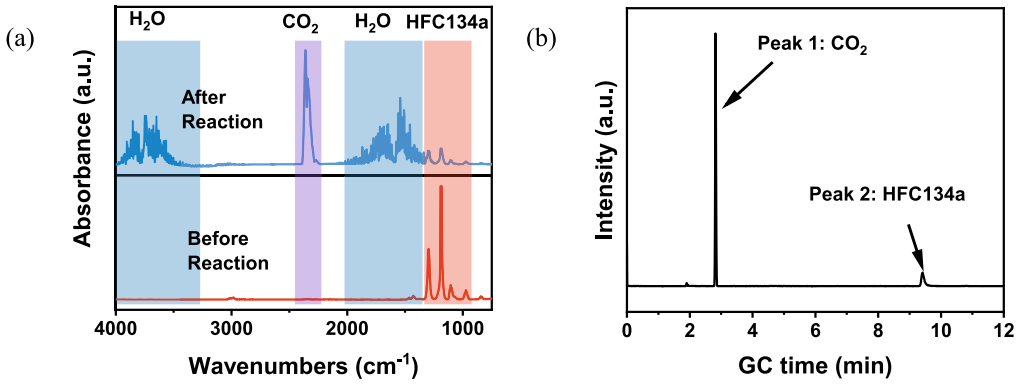

Fig. 7. (a) FTIR results before and after the reaction (b) MS results of the gases after the reaction.

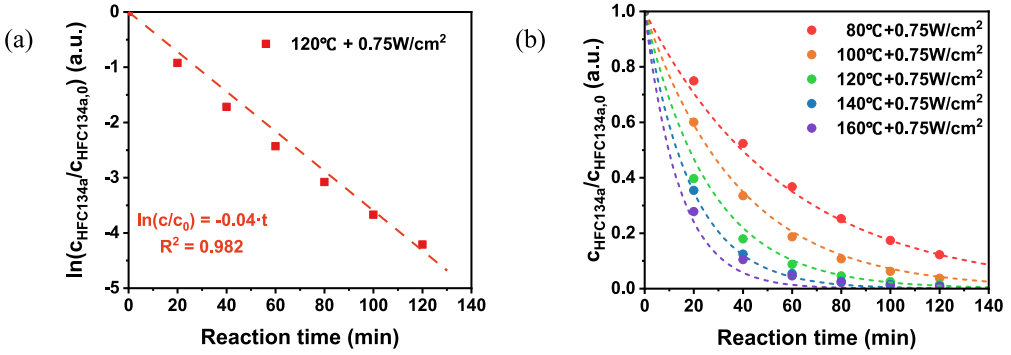

Fig. 8. (a) Relationship between $\ln(c_{HFC134a}/c_{HFC134a,0})$ and the reaction time at 120 °C; (b) Comparison of the model calculation values with experimental values.

descent method. As shown in Fig. 6b, the calculation values by the apparent kinetics model (dashed line) were consistent with the experimental values (scatter plot). Compared with the activation energy of thermal decomposition (278.7 kJ/mol) [27], the activation energy of photo-thermal synergistic catalysis (22.3 kJ/mol) is very small, indicating that photo-thermal synergistic catalysis can greatly reduce the activation energy of the reaction.

Fig. 9 shows the degradation curves with different light intensities under 120 °C. The degradation rate gradually increased with increasing light intensity. When the light intensity was bigger than 0.9 W/cm^2, the increasing trend of reaction rate with light intensity slowed down, which was probably due to the saturation of light absorption. According to the reference [28], the reaction rate constant k has a power-law relationship with light intensity I:

$$k = C_0 \cdot I^{\alpha} \tag{5}$$

Therefore, under constant temperature conditions, the relationship between the reaction rate constant and light intensity can be derived, as shown in Fig. 9b.

It is assumed that the variation pattern of the reaction rate with light intensity does not vary with temperature in the range of 80~160 °C. On the basis of the fitting of various factors, the reaction kinetics equation is obtained as follows:

$$c_{HFC134a} = c_{HFC134a,0} \cdot \exp\left(-1.2038 \cdot I^{0.6229} \cdot A_0 \cdot \exp\left(-E_a/RT\right)\right) \tag{6}$$

where, I is light intensity of Xe lamp (W/cm^2), T is temperature of reaction device (K), t is reaction time (min), R = 8.314 J/(mol·K), A_0 = 35.12 min^{-1}, E_a = 22.3 kJ/mol.

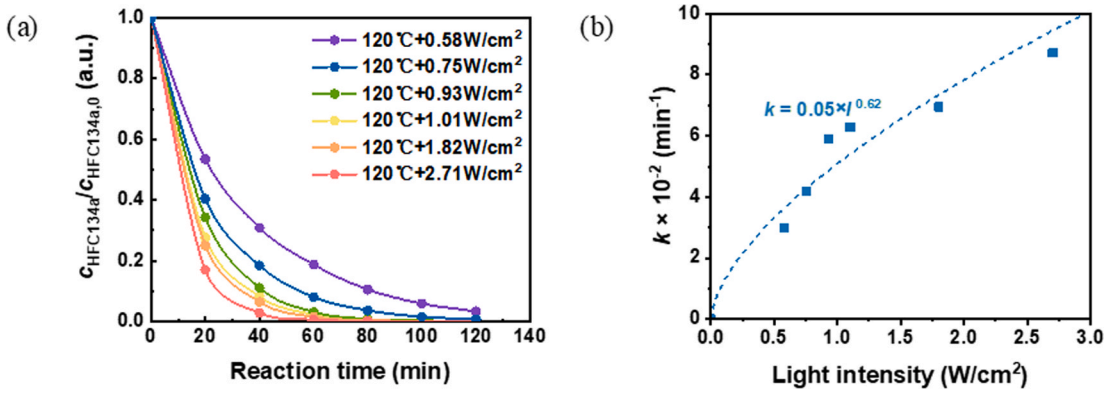

Fig. 9. (a) Degradation of HFC134a under different light intensities; (b) Relationship between light intensity and reaction rate constant.

3.3. Analysis of catalyst lifespan and deactivation mechanism

To verify the persistence of catalyst activity, the same catalyst was repeatedly tested for 20 cycles at 120 °C and 0.75 W/cm^2 light (the gas was replaced after each experiment and the catalyst was not replaced). The test results are shown in Fig. 10a. The relationship between the reaction rate constant and the number of cycles is shown in Fig. 10b. The activity of the catalyst decreased significantly after 20 reaction cycles, which indicated that the catalyst had be corroded during the reaction cycles.

The anatase TiO_2 catalyst powder before the reaction was named as AT-R0 in this paper. After 10 reaction cycles at 120 °C under the light of 0.75 W/cm^2, the obtained powder was named as AT-R10, and the powder after 20 cycles was named as AT-R20.To clarify the difference in the catalyst before and after the reaction, AT-R0, AT-R10 and AT-R20 were tested through XRD, XPS and SEM.

Fig. 11a shows the XRD patterns of the catalyst powder before and after the reaction. The peaks at 25.4°, 37.9°, and 48.2° found in the XRD patterns of AT-R0, AT-R10 and AT-R20 were indexed to the characteristic peaks of anatase TiO_2. Meanwhile, peaks at 23.40° and 33.34° only appeared in the XRD patterns of AT-R10 and AT-R20, which were the characteristic peaks of $TiOF_2$ (PDF#01–077-0132). The proportion of $TiOF_2$ increased obviously after several cycles, while the proportion of anatase TiO_2 decreased. The results suggested that part of the anatase TiO_2 changed to $TiOF_2$ after the degradation reaction, which may be due to the HF corrosion.

XPS spectra shows the content of different kinds of chemical bonds in the catalyst samples. Fig. 11b shows the Ti2p spectra of AT-R0, AT-R10 and AT-R20. Three peaks at 458.8 eV, 459.3 eV and 464.4 eV were detected. The characteristic peaks near 458.8 eV and 464.4 eV are due to the $2p_{3/2}$ and $2p_{1/2}$ orbitals of TiO_2, respectively, and the characteristic peaks near 459.3 eV are due to the $2p_{1/2}$ orbital of $TiOF_2$[29]. The results showed that only peaks belonging to TiO_2 appeared in the Ti2p spectrum before the reaction. With the increasing number of cycles, the peak belonging to $TiOF_2$ gradually increased, and the binding energy of $Ti2p_{1/2}$ also increased. The F1s spectra results are shown in Fig. 11c. The peaks near 684.4 eV were due to metal-fluorine bonds instead of organic fluorine bonds, indicating that the bonding form of fluorine on the catalyst after reaction was metal fluoride bond. The XPS results were consistent with the conclusions obtained by XRD analysis and further confirmed that $TiOF_2$ was created after the reaction.

Micromorphologies for catalysts were obtained by SEM. The morphology of the catalyst was extremely different after the reaction as shown in Fig. S6. AT-R0 consisted of nanospheres with a diameter of 20~50 nm (Fig. S6a). However, more bulks like morphology appeared in AT-R10 and AT-R20 (Fig. S6b, Fig. S6c). On the basis of the results of EDX-mapping of AT-R10 and AT-R20 (Fig. S7, Fig. S8), these bulks may be grains of $TiOF_2$ transformed by the reaction of the original nano-TiO_2. The EDS results are shown in Fig. S6d, e, f. The mass fractions of F in AT-R10 and AT-R20 were 23.1 % and 43.4 %, respectively, which also indicated the creation of $TiOF_2$.

It could be concluded that the conversion of TiO_2 to $TiOF_2$ is a characteristic of HFC134a degradation. However, since the reactor was evacuated after allowing the reaction to rest for a while in the cyclic tests, whether the conversion of TiO_2 to $TiOF_2$ is an essential mechanism for the reaction to proceed is still not clear.

For further investigation, the amount of catalyst used was adjust. Experiments were conducted under the conditions of 120 °C and 0.75 W/cm^2, using 500 mg and 100 mg of catalyst, respectively. The results were showed in Fig. 12a. No significant difference in reaction rates was observed. For the 100 mg catalyst, we conducted experiments to retrieve the catalyst immediately after one reaction or after allowing it to rest for more than 1-hour post-reaction. The XRD results, as shown in Fig. 12b, indicate that less $TiOF_2$ was generated when the catalyst was quickly removed, whereas more $TiOF_2$ formed as the resting time increased after the reaction. These results indicated that TiO_2 remained a photocatalyst rather than a reactant. Its photocatalytic reaction and corrosion reaction were probably two independent processes.

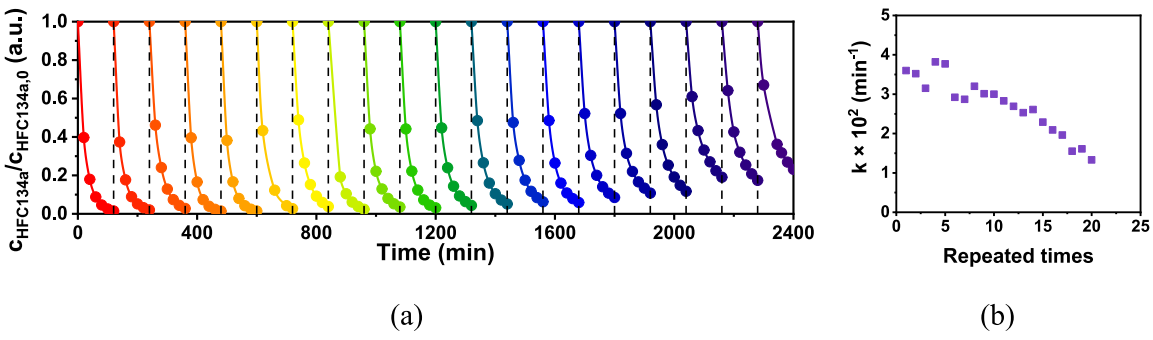

Fig. 10. (a) R134a degradation for 20 cycles; (b) Relationship between repeated times and reaction rate constant.

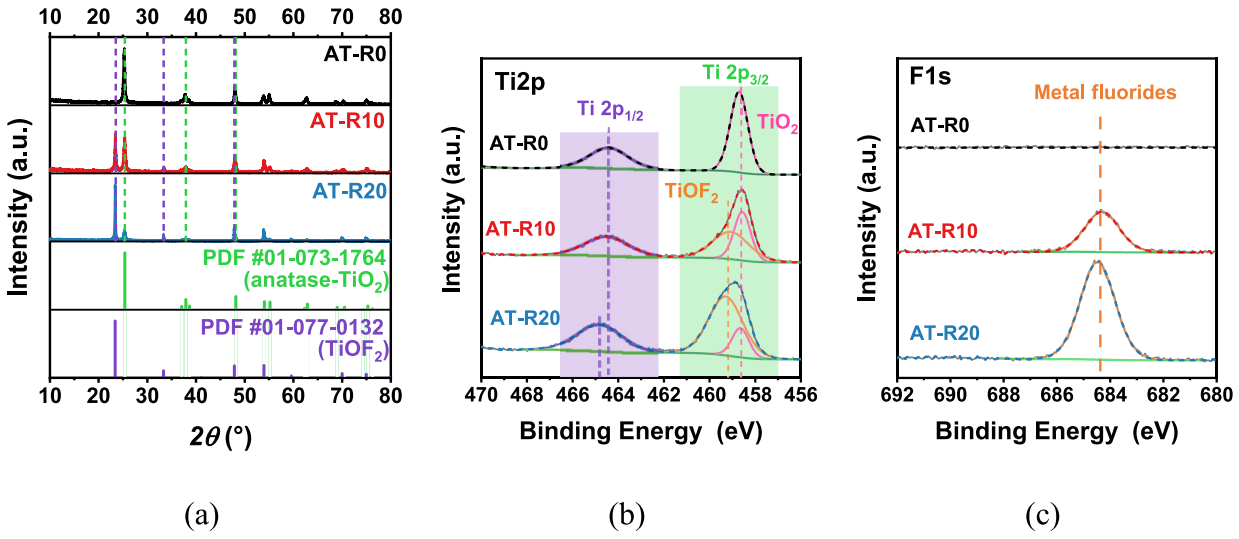

Fig. 11. (a) XRD patterns; (b) Ti2p XPS spectra; (c) F1s XPS spectra of catalysts after 0 cycles (AT-R0), 10 cycles (AT-R10) and 20 cycles (AT-R20).

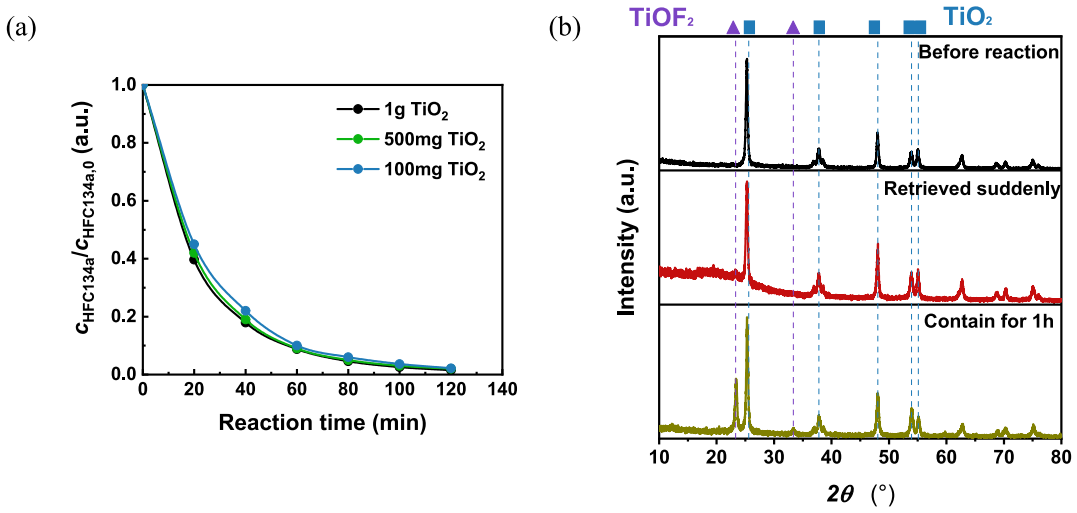

Fig. 12. (a) activities of different amount of TiO_2 and (b) influence of retrieve time.

Another evidence is, when quartz glass was initially used as the light window, after just a few reactions, the quartz window changed from clear and transparent to significantly blurred, as shown in Fig. S9. This is also likely due to HF corrosion, further indicating that HF was generated as a product in the reaction and not directly as a result of HFC134a reacting with TiO_2.

In conclusion, sufficient amounts of $TiOF_2$ were generated during the degradation reaction to reduce the catalyst activity, which was due to the corrosion of HF.

3.4. Overall reaction equation of photo-thermal synergistic catalysis degradation

On the basis of the results of experiments and catalyst characterization, it can be concluded that the degradation of HFC134a achieved complete mineralization, and 1.5 times oxygen was consumed after the degradation of HFC134a. Meanwhile, the catalyst was corroded by HF in the reaction process and became $TiOF_2$. Therefore, the overall reaction of photo-thermal synergistic catalysis degradation can be formulated as Eq. (7), and the reaction also can be composed of two steps as Eqs. (8) and (9).

$$C_2H_2F_4 + 1.5O_2 + 2TiO_2 = 2CO_2 + H_2O + 2TiOF_2 \quad (7)$$

$$C_2H_2F_4 + 1.5O_2 + H_2O = 2CO_2 + 4HF \quad (8)$$

$$2HF + TiO_2 = TiOF_2 + H_2O \quad (9)$$

Fig. 13a shows the variation of c_{H2O} during HFC134a degradation under 120 °C and 0.75 W/cm^2 light, which was tested by a DP70C high temperature dew point sensor. Since no water was added at the beginning of the reaction, the water used in Eq. (8) may come from the products in Eq. (9), suggesting that the concentration of water in the reaction system increased with the degradation of HFC134a.

In the cyclic tests mentioned in 3.3, it could be assumed that all HF produced from HFC134a fully reacted with TiO_2. The relationship between photocatalytic activity k and the cumulative amount of degraded HFC134a was shown in Fig. 13b. Assuming all HF generated by HFC134a reacted with the catalyst, and $TiOF_2$ showed no activity on HFC134a degradation, the theoretically predicted relationship between k and cumulative HFC134a degradation was also illustrated in Fig. R4. The experimental data aligns closely with the predicted results, further validating the overall reaction equation.

The overall reaction equation illustrateed that the presence of the corrosion reaction allowed HF-derived hydrogen to convert into water, which stabilized the reaction even under conditions with nearly no

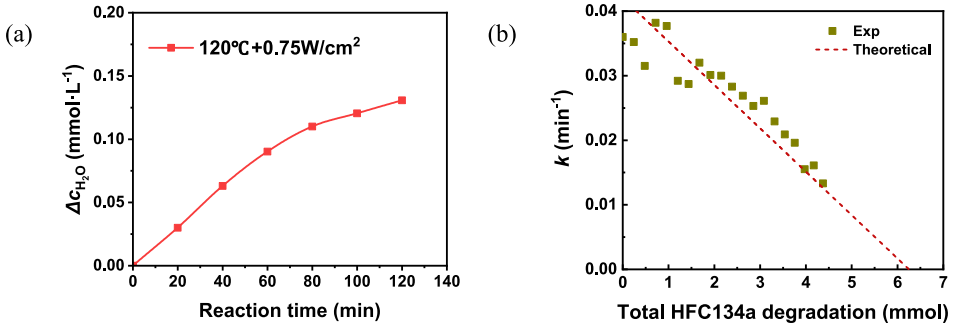

Fig. 13. (a)c_{H2O} during HFC134a degradation under 120 °C and 0.75 W/cm^2 light; (b) relationship between k and cumulative HFC134a degradation.

initial water. This understanding of the reaction mechanism not only aided in recognizing the characteristics of photothermal catalytic degradation of HFCs but also provided insights for future efforts to enhance reaction rates and minimize the impact of HF. Strategies such as improving mass transfer to prevent HF from reacting with the catalyst or introducing sacrificial agents more reactive with HF could be considered.

4. Conclusions

This paper presented a novel photo-thermal synergistic catalysis method for the degradation of waste HFCs, demonstrating superior performance over traditional thermocatalysis and photocatalysis methods. The experimental results revealed that complete mineralization of HFC134a can be achieved under mild reaction conditions, making this method a promising technology for waste HFC destruction. The effect of different catalysts, including anatase TiO_2, on the degradation efficiency was measured, with anatase TiO_2 showing the highest catalytic performance. The impact of reaction conditions, such as O_2 concentration, temperature, and light intensity, on degradation efficiency was also thoroughly investigated. Kinetic analysis showed that the degradation of HFC134a follows first-order kinetics, with an activation energy of 22.3 kJ·mol^{-1}, which was much lower than that of thermal decomposition methods. Catalyst characterization tests revealed the formation of $TiOF_2$ during degradation, which was caused by HF creation and affected catalytic activity. The anticorrosion and regeneration for long-term catalyst stability should also be focused. The proposed method provided a viable and efficient alternative for the sustainable destruction of waste HFCs, with potential for application in industrial-scale processes.

Declaration of competing interest

The authors declare that they have no known competing financial interests or personal relationships that could have appeared to influence the work reported in this paper.

Acknowledgement

This work was supported by the National Natural Science Foundation of China (52236003, 52176011) and the Creative Seed Fund of Shanxi Research Institute for Clean Energy, Tsinghua University.

Appendix A. Supplementary data

Supplementary data to this article can be found online at https://doi.org/10.1016/j.applthermaleng.2025.126211.

Data availability

Data will be made available on request.

References

[1] United Nations Environment Programme (UNEP), Montreal Protocol on Substances that Deplete the Ozone Layer, 1987. Available online: https://ozone.unep.org/treaties/montreal-protocol.
[2] A.R. Ravishankara, S. Solomon, A.A. Turnipseed, et al., Atmospheric lifetimes of long-lived halogenated species, Science 259 (5092) (1993) 194–199, https://doi.org/10.1126/science:259.5092.194.
[3] J. Franklin, The atmospheric degradation and impact of 1,1,1,2-tetrafluoroethane (hydrofluorocarbon 134a), Chemosphere 27 (8) (1993) 1565–1601, https://doi.org/10.1016/0045-6535(93)90251-Y.
[4] P. Purohit, L. Höglund-Isaksson, Global emissions of fluorinated greenhouse gases 2005–2050 with abatement potentials and costs, Atmos. Chem. Phys. 17 (7) (2017) 2795–2816, https://doi.org/10.5194/acp-17-2795-2017.
[5] E.A. Heath, Amendment to the Montreal Protocol on Substances that Deplete the Ozone Layer (Kigali Amendment), Int. Legal Materials 56 (1) (2017) 193–205, https://doi.org/10.1017/ilm.2016.2.
[6] N.D. Miranda, P.G. Palafox-Alcantar, R. Khosla, M.D. McCulloch, Metrics for the emissions of F-gas refrigerants, Sustainable Energy Technol. Assess. 58 (2023) 103348, https://doi.org/10.1016/j.seta.2023.103348.
[7] US Environmental Protection Agency. ODS Destruction in the United States and Abroad. 2018. Available online: https://www.epa.gov/sites/default/files/2018-03/documents/ods-destruction-in-the-us-and-abroad_feb2018.pdf.
[8] Y. Takita, M. Ninomiya, R. Matsuzaki, H. Wakamatsu, H. Nishiguchi, T. Ishihara, Decomposition of chlorofluorocarbons over metal phosphate catalysts Part I. Decomposition of CCl_2F_2 over metal phosphate catalysts, Phys. Chem. Chem. Phys. 1 (1999) 2367–2372, https://doi.org/10.1039/A809967G.
[9] P.M. Lemieux, J.V. Ryan, C. Bass, et al., Emissions of trace products of incomplete combustion from a pilot-scale incinerator secondary combustion chamber, J. Air Waste Manag. Assoc. 46 (4) (1996) 309–316, https://doi.org/10.1080/10473289.1996.10467465.
[10] H. Ueno, Y. Iwasaki, S. Tatsuichi, et al., Destruction of chlorofluorocarbons in a cement kiln, J. Air Waste Manag. Assoc. 47 (11) (1997) 1220–1223, https://doi.org/10.1080/10473289.1997.10464068.
[11] C. Lamb, B. Dellinger, M. Wagner, et al., Incinerability of halons and HCFCs: theoretical calculations of DRE and ozone-depleting or global-warming gases, Environ. Eng. Sci. 27 (2010) 7, https://doi.org/10.1089/ees.2009.0393.
[12] S.A. Roh, W.H. Kim, D.S. Jung, et al., Thermal destruction of HFC-134a in pilot-, and full-scale gasification systems, J. Energy Inst. 92 (6) (2019) 1842–1851, https://doi.org/10.1016/j.joei.2018.11.008.
[13] T.U. Han, B.S. Yoo, Y.M. Kim, et al., Catalytic conversion of 1,1,1,2-tetrafluoroethane (HFC-134a), Korean J. Chem. Eng. 35 (8) (2018) 1611–1619, https://doi.org/10.1007/s11814-018-0051-7.
[14] C.A. Swamidoss, M. Sheraz, A. Anus, et al., Effect of Mg/Al_2O_3 and calcination temperature on the catalytic decomposition of HFC-134a, Catalysts 9 (3) (2019) 270, https://doi.org/10.3390/catal9030270.
[15] S. Jeong, G.L. Sudibya, J.-K. Jeon, Y.-M. Kim, C.M.A. Swamidoss, S. Kim, The use of a γ-Al_2O_3 and MgO mixture in the catalytic conversion of 1,1,1,2-tetrafluoroethane (HFC-134a), Catalysts 9 (2019) 901, https://doi.org/10.3390/catal9110901.
[16] B. Sangchakr, T. Hisanaga, K. Tanaka, Photocatalytic degradation of 1,1-difluoroethane (HFC-152a), Chemosphere 36 (9) (1998) 1985–1992, https://doi.org/10.1016/S0045-6535(97)10083-2.
[17] S. Kutsuna, K. Takeuchi, T. Ibusuki, Adsorption and reaction of trichlorofluoromethane on various particles, J. Atmos. Chem. 14 (1–4) (1992) 1–10, https://doi.org/10.1007/BF00115218.
[18] D.J. Wylie, R.P. Cooney, J.M. Seakins, et al., Spectroscopic studies of the adsorption and reactions of chlorofluorocarbons (CFC-11 and CFC-12) and hydrochlorofluorocarbon (HCFC-22) on oxide surfaces, Vibrational Spectrosc. 9 (3) (1995) 245–256, https://doi.org/10.1016/0924-2031(95)00016-N.
[19] K. Tennakone, K.G.U. Wijayantha, Photocatalysis of CFC degradation by titanium dioxide, Appl. Catal. B: Environ. 57 (1) (2005) 9–12, https://doi.org/10.1016/j.apcatb.2004.10.004.
[20] J. Li, S. Mo, X. Ding, L. Huang, X. Zhou, Y. Fan, Y. Zhang, M. Fu, Q. Xie, D. Ye, Hollow cavity engineering of MOFs-derived hierarchical MnO_x structure for highly efficient photothermal degradation of ethyl acetate under light irradiation, Chem. Eng. J. 464 (2023) 142412, https://doi.org/10.1016/j.cej.2023.142412.

[21] C. Wang, H. Ma, Y. Tian, A. Jiao, M. Zhang, L. Zheng, S. Li, M. Chen, Polymeric layered semiconductor-supported black nano-sandwiches with synergistic photo-thermal catalysis for efficient wastewater decontamination, Chem. Eng. J. 446 (2022) 136977, https://doi.org/10.1016/j.cej.2022.136977.
[22] L. Xu, Y. Ren, Y. Fu, M. Liu, F. Zhu, M. Cheng, J. Zhou, W. Chen, K. Wang, N. Wang, N. Li, Strong photo-thermal coupling effect boosts CO_2 reduction into CH_4 in a concentrated solar reactor, Chem. Eng. J. 468 (2023) 143831, https://doi.org/10.1016/j.cej.2023.143831.
[23] Y. Shen, Y. Shi, Z. Chen, S. Zhang, K. Chen, X. Luo, F. Guo, G. Wang, W. Shi, Core-shell nanoconfinement: nanoreactors for directional electron migration in photothermal-assisted photocatalytic hydrogen production, Chem. Eng. J. 484 (2024) 149607, https://doi.org/10.1016/j.cej.2024.149607.
[24] Y. Zhang, J. Shi, Z. Huang, et al., Synchronous construction of CoS_2 in-situ loading and S doping for g-C_3N_4: enhanced photocatalytic H_2-evolution activity and mechanism insight, Chem. Eng. J. 401 (2020) 126135, https://doi.org/10.1016/j.cej.2020.126135.
[25] C. Pan, Y. Zhu, New type of $BiPO_4$ oxy-acid salt photocatalyst with high photocatalytic activity on degradation of dye, Environ. Sci. Technol. 44 (14) (2010) 5570–5574, https://doi.org/10.1021/es101223n.
[26] Y. Xu, K. Zhang, X. Dai, et al., Thermal decomposition and oxidative decomposition mechanism of HFC-134a by experimental and DFT method, J. Therm. Sci. 33 (2024) 1990–2003, https://doi.org/10.1007/s11630-024-1981-5.
[27] A. Iizuka, H. Ishizaki, A. Mizukoshi, M. Noguchi, A. Yamasaki, Y. Yanagisawa, Simultaneous decomposition and fixation of F-gases using waste concrete, Ind. Eng. Chem. Res. 50 (21) (2011) 11808–11814, https://doi.org/10.1021/ie201727j.
[28] K. Wang, H. Tsai, Y. Hsieh, The kinetics of photocatalytic degradation of trichloroethylene in gas phase over TiO_2 supported on glass beads, Appl. Catal. B: Environ. 17 (4) (1998) 313–320, https://doi.org/10.1016/S0926-3373(97)00099-4.
[29] Y. Chen, X. Wang, Z. Zeng, et al., Towards molecular understanding of surface and interface catalytic engineering in TiO_2/$TiOF_2$ nanosheets photocatalytic antibacterial under visible light irradiation, J. Hazard. Mater. 465 (2024) 133429, https://doi.org/10.1016/j.jhazmat.2024.133429.